

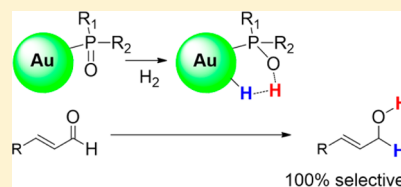
Air-Stable Gold Nanoparticles Ligated by Secondary Phosphine Oxides for the Chemoselective Hydrogenation of Aldehydes: Crucial Role of the Ligand

Israel Cano, Andrew M. Chapman, Atsushi Urakawa, and Piet W. N. M. van Leeuwen*

Institute of Chemical Research of Catalonia (ICIQ), 43007 Tarragona, Spain

S Supporting Information

ABSTRACT: The synthesis of air-stable and homogeneous gold nanoparticles (AuNPs) employing *tert*-butyl(naphthalen-1-yl)phosphine oxide as supporting ligand is described via NaBH_4 reduction of a Au(I) precursor, [(*tert*-butyl(naphthalen-1-yl)phosphine oxide)AuCl] $_2$. This highly reproducible and simple procedure furnishes small (1.24 ± 0.16 nm), highly soluble nanoparticles that are found to be highly active catalysts for the hydrogenation of substituted aldehydes, giving high conversions and chemoselectivities for a wide variety of substrates. In addition to catalytic studies the role of the novel stabilizer in the remarkable activity and selectivity exhibited by this system was interrogated thoroughly using a wide range of techniques, including ATR FT-IR, HRMAS NMR, XPS, and EDX spectroscopy. In particular, isotopic labeling experiments enabled us to probe the coordination mode adopted by the SPO ligand bound to the nanoparticle surface by ATR FT-IR spectroscopy. In combination with a series of control experiments we speculate that the SPO ligand demonstrates ligand–metal cooperative effects and plays a seminal role in the heterolytic hydrogenation mechanism.



INTRODUCTION

Secondary phosphine oxides (or SPOs) form an interesting, yet relatively underexploited, class of phosphorus ligands.^{1,2} It is well-known that the free ligands exist in equilibrium between the pentavalent phosphine(V) oxide and the trivalent phosphinous(III) acid and that, in the vast majority of cases, the equilibrium is heavily in favor of the P(V) species.³ It is also well established that once coordinated (via P) to a suitable transition metal, they coordinate as the phosphinous(III) acid tautomer⁴ and the resulting complexes have been shown to exhibit some interesting reactivity in which the pendant OH group may act as an acid,⁵ as a directing group,⁶ or as a pendant base.⁷ Such ligand–metal cooperative effects have been widely utilized in a variety of catalysis: for example, in Ru-catalyzed hydrogenation, where such reactivity is particularly notorious.⁸ In that regard, we have already shown that the self-assembly of SPOs into an anionic bidentate, binuclear Rh(III) chelate serves as a unique system for metal-catalyzed transfer hydrogenation of ketones in which ligand–metal cooperation plays a formative role. Given our longstanding interest in the use of phosphorus ligands as nanoparticle stabilizers, we were keen to explore the utility of SPO ligands in that regard. We recently reported a series of Ru nanoparticles stabilized by SPOs and demonstrated that they function as active hydrogenation catalysts for arenes. What is more, we demonstrated the participation of P–O groups in H_2/D_2 exchange reactions by IR and solid-state ^2H NMR spectroscopy, which was speculated to involve the heterolytic cleavage of dihydrogen across surface Ru and P–O surface groups.⁹ In this work we have extended this approach to the synthesis of stable and homogeneous gold nanoparticles (AuNPs) stabilized by an SPO. An extremely diverse range of molecules have already been used to stabilize AuNPs: for

example, thiols,¹⁰ polymers,^{11–13} carbenes,¹⁴ amines,^{15,16} thioethers,¹⁶ alkynes,¹⁷ and even primary,¹⁸ secondary,^{19,20} and tertiary phosphines,^{11,20,21} but to the best of our knowledge this is the first case which describes the use of SPOs as stabilizing ligands for AuNPs and, more importantly, the first that aims to investigate the role of these ligands in catalysis.²² Although a multitude of catalysis has been demonstrated with supported Au materials in addition to oxidation,²³ there is very little precedent for catalysis, hydrogenation catalysis in particular, with *homogeneous* Au nanoclusters. We demonstrate here through extensive characterization and experimentation that the SPO plays a crucial role in giving the highest activity and selectivity in the catalytic hydrogenation of α,β -unsaturated aldehydes to date by nanoparticles.

RESULTS AND DISCUSSION

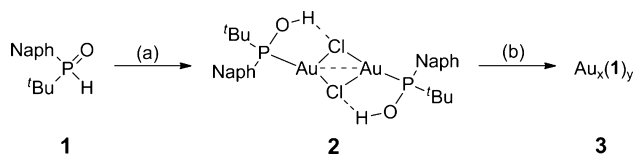
Synthesis and Characterization of SPO-Stabilized Au Nanoparticles. The synthetic methodologies available to access gold nanoparticles almost always involve the chemical reduction of a Au(III) or Au(I) precursor by borohydride and, in general, are based on the original procedure developed by Brust et al. used for the synthesis of well-defined gold clusters,¹⁰ although additional methodologies have been developed that employ neutral reducing agents such as 9-BBN²⁴ and B_2H_6 .^{21b} The common procedure utilized by Hutchison^{21c} and others^{21d} for the preparation of phosphine-stabilized AuNPs requires phase-transfer conditions in order to solubilize HAuCl_4 hydrate and permits the initial reduction from Au(III) to Au(I) by

Received: November 6, 2013

Published: January 20, 2014

triphenylphosphine. When we used SPOs in an analogous procedure, we noted that the anticipated equivalent of $R_2P(O)OH$ is generated as Au(III) is reduced to Au(I) in the initial step, forming the expected Au(I) phosphine complex. In the interest of simplicity, we chose to avoid the possible complication to the system that may arise from the presence of the $R_2P(O)OH$ acid byproduct. In order to circumvent this potential issue, we opted for an alternative route²⁰ starting from preformed Au(I) complexes which are formed almost quantitatively from the reaction of the appropriate SPO with [(tth)AuCl] (Scheme 1). After an initial screening of some of

Scheme 1. Formation of 2 from 1 and Subsequent Reduction of 2 to AuNPs 3^a



^aReagents and conditions: (a) 0.98 equiv of [(tth)AuCl], DCM, 25 °C, 5 h; (b) 16 equiv of NaBH₄, THF/H₂O (1.4/1), 0–25 °C, 15 h.

the SPOs utilized in our previous studies,⁹ we found that **1** consistently yielded highly soluble, small (vide infra) nanoparticles. The dimeric structure of the Au(I) precursor **2** in the solid state is almost identical with that of the previously reported Au(I)-SPO complex [Ph₂P(OH)AuCl]₂.²⁵

Treatment of a cooled²⁶ THF solution of **2** with a freshly prepared solution of NaBH₄ in water resulted in an immediate color change from colorless to deep red-brown and vigorous gas evolution. After the reaction mixture was warmed to ambient temperature with rapid stirring overnight, the organic-soluble fraction containing the nanoparticles was extracted and purified by precipitation (see the Supporting Information). We have tried to investigate the reaction of **2** and NaBH₄ in more detail, but no conclusive results on the coproducts could be obtained (section 4, Supporting Information). The procedure consistently furnished monodisperse nanoparticles of size ca. 1.24(0.16) nm (Figure 1) which were highly soluble in apolar

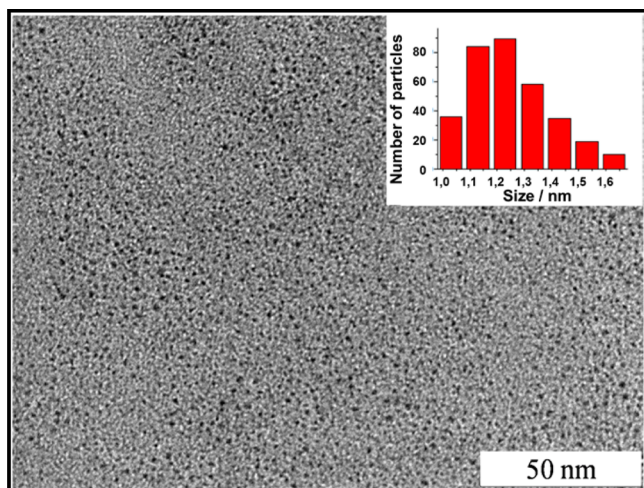


Figure 1. Representative TEM image of AuNPs **3** and size distribution determined from TEM images by counting >300 nontouching particles obtained from images captured from distinct quadrants of the grid.

organic solvents (hexane, diethyl ether, toluene, and dichloromethane) but insoluble in MeOH, which facilitated purification by reprecipitation from ether/MeOH. The purified nanoparticles were fully characterized by EDX, XPS, HRMAS, and solid-state NMR, TEM, ATR-IR, UV-vis, TGA, XRD, and elemental analysis. The procedure was repeated many times and gave very consistent size distributions by TEM and identical UV-vis, NMR, and ATR FT-IR spectra.

The UV-vis spectrum of **3** (Figure S6, Supporting Information) contains no surface plasmon band, which is generally accepted to confirm that there is not a detectable number of nanoparticles greater than 2 nm in size present in the bulk sample in solution.^{21c,27} Furthermore, no trace of **1** or **2** was observed in the UV-vis spectrum, indicating that they are effectively removed by washing,²⁸ and this was confirmed by comparison of the XPS,²⁹ UV-vis, and ³¹P{¹H} and ¹H NMR spectra of **1**–**3**. No significant chemical information could be extracted from the energy of the C, O, or P XPS peaks (Figures S2–S4, Supporting Information). However, a significant drop in the Au(4f) binding energy (0.85 eV) was observed in **3** in comparison to that of **2** and this drop corresponds almost exactly to that of related Au acetylide clusters.¹⁷ The drop in binding energy is to be expected, considering that while **2** is 100% Au(I), in **3** a mixture of Au(I) and Au(0) is expected. The XRD pattern measured for **3** showed expectedly broad features¹⁷ due to the nanostructure yet presented structural regularity of bulk Au (Figure S19, Supporting Information). Elemental analysis of **3** gives a Au content of ca. 46%, which is supported by TGA³⁰ (ca. 47%) and EDX (ca. 47%). Elemental analysis, XPS (Figure S1, Supporting Information), EDX (Figure S5, Supporting Information), and MALDI show the absence of chloride in the nanoparticles. TGA, the fastest method for analysis, shows that the reproducibility is high, although we do not obtain a single MNP, as has been reported for some Au and AgNP recipes.³¹ The techniques applied here tell us that the average composition of the AuSPO nanoparticles is Au₅₀(**1**)_{30–33}. We have not been able to identify such a large species in MALDI-TOF analysis, but for both cations and anions we see broad ranges of lower MW species between 2500 and 9000 Da. Cations and anions give almost the same spectrum, showing that there is no Cl present. Low-MW species are Au(**1**)₂, Au₂(**1**)₂, etc., which also show no chloride. Anions and cations are monocharged, and the differences between the MWs are always those of Au and **1**. All signals between 3000 and 8000 can be assigned to a specific cluster Au_x(**1**)_y (see the Supporting Information). No inclusion of degraded solvent was observed in this instance as was found for Ru.³²

There is significant debate in the literature concerning the solution NMR spectra of metal nanoparticles, which are expected to be broad if observable, due to slow molecular tumbling, Knight-shift-induced line broadening, exchange-induced line-shape effects, different coordination sites, etc.³³ In spite of these expectations, in some cases sharp signals typical of mononuclear, homogeneous compounds have been reported, even in the case where the metal is known to produce a strong Knight shift (Pd).³⁴ In one case of particular relevance to this work, it has been elegantly demonstrated that such sharp ³¹P NMR signals of the triphenylphosphine ligands of Schmid's Au₅₅ cluster are in fact attributable to the unavoidable dissociation of mononuclear [PPh₃AuCl] units.³⁵ In our case, the solution-phase NMR spectra of **3** revealed only very broad aromatic and aliphatic signals in the ¹H NMR spectrum and

only a very broad signal by $^{31}\text{P}\{^1\text{H}\}$ NMR spectroscopy. It has been shown that solution-phase NMR spectra of phosphine ligands bound to AuNPs is improved at low temperatures,³⁶ yet in our case variable-temperature experiments revealed that the ^1H NMR line widths were only very marginally affected in the range -90 to $+100$ °C, while the $^{31}\text{P}\{^1\text{H}\}$ NMR spectra were essentially unchanged over the same range. In spite of these broad ^1H NMR signals, the chemical shifts of these two groups of signals corroborate the expectation of both aromatic (naphthyl) and aliphatic (*tert*-butyl) protons.³⁷ High-Resolution Magic Angle Spinning (HRMAS) NMR spectroscopic techniques have been used to reduce the line-broadening phenomenon frequently encountered with NMR spectroscopy of nanoparticles. We ourselves have made use of HRMAS NMR spectroscopy to observe the signals of phosphine ligands coordinated to Ru nanoparticles and were able to ascertain, on the basis of chemical shift, that aryl phosphines are hydrogenated on the nanoparticle surfaces.³² In this case, while we found little improvement in the appearance of the ^1H HRMAS NMR spectra of **3** (Figure S16, Supporting Information),³⁸ the effect on the $^{31}\text{P}\{^1\text{H}\}$ NMR resonances is dramatic (Figure 2).

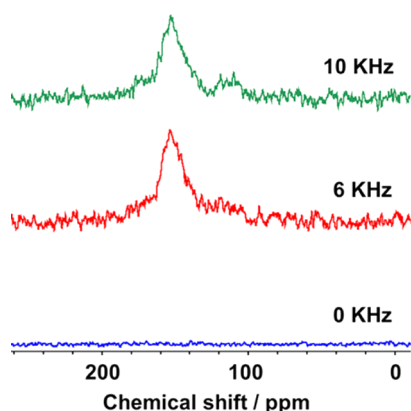


Figure 2. Effect of spinning rate on the HRMAS $^{31}\text{P}\{^1\text{H}\}$ NMR spectrum of **3**.

Although the $^{31}\text{P}\{^1\text{H}\}$ NMR resonance under normal conditions is extremely broad (Figure S17, Supporting Information), in the temperature range -90 to $+100$ °C, the approximate chemical shift corresponds well to that observed in the HRMAS experiment. Furthermore, the HRMAS spectrum acquired without spinning gave no observable signal. With a spinning rate of 10 kHz, two signals are clearly resolved (Figure 2), neither of which corresponds to **1** or **2**. What is more, the chemical shifts of these two signals (a major signal at 154 ppm and a minor signal at 114 ppm, respectively) correspond almost exactly with those observed in the solid-state $^{31}\text{P}\{^1\text{H}\}$ NMR experiment (Figure 3). These findings suggest that there are two distinct, unequally populated phosphine environments in **3**. Although it is not possible to assign these signals to any particular coordination mode or indeed chemical environment as yet, various chemically distinct phosphine environments would be predicted for metal nanoparticles with anisotropic surface sites (edges, faces, and corners, for example).

IR Studies. Given the relatively limited information that can be extracted from the NMR spectra of nanoparticles, we find ATR FT-IR to be an extremely useful spectroscopic tool. It is very sensitive, fast, and (in this case in particular) highly diagnostic when attempting to identify particular bonding

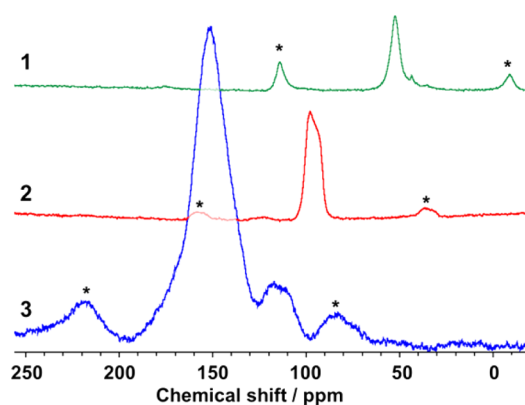


Figure 3. Comparison of the solid-state $^{31}\text{P}\{^1\text{H}\}$ NMR spectra of **1–3**. Asterisks denote spinning sidebands.

motifs. We were very keen to exploit these characteristics in identifying the bonding of **1** bound in **3**. Comparison of the ATR FT-IR spectra of **3** with those of **1** and **2** gives some initial insight (Figure 4). First, it is clear that no $(\text{P})\text{O}\text{H}$ ³⁹

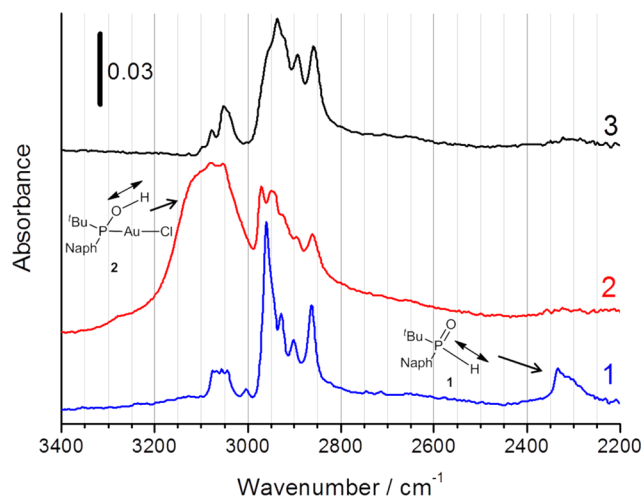


Figure 4. ATR FT-IR spectra of **1–3** in the region of P–H, C–H, and O–H stretching vibrations.

stretching band is observable in **3**, and in fact this region of the spectrum closely resembles that of free ligand **1**. Second, the P–H⁴⁰ stretching absorption in **1** located at 2340 cm^{-1} is clearly absent or is dramatically shifted in **3**, suggesting that **1** is bound as $\text{Au}\text{P}(\text{O})\text{R}_2$ in **3**.

In order to identify the expected $\text{P}=\text{O}$ stretching absorption that would be expected to accompany this coordination mode, we prepared the ^{18}O -labeled nanoparticles **3- ^{18}O** in order to observe an isotopic shift in the anticipated $\text{P}=\text{O}$ band. According to the harmonic oscillator approximation, the diatomic systems of $\text{P}\text{--}^{16}\text{O}$ and $\text{P}\text{--}^{18}\text{O}$ would result in a roughly 3.7% decrease in stretching frequency upon isotopic substitution by ^{18}O . The magnitude of the isotopic shift observed in the $\text{P}=\text{O}$ ⁴¹ stretch between **1** and **1- ^{18}O** was ca. 37 cm^{-1} , which is in good agreement with the expected change. On the other hand, close inspection of the spectra of **3** and **3- ^{18}O** (Figure 5) reveals that there are marked changes in the region where P–O and $\text{P}=\text{O}$ stretching bands are expected to appear according to **1** and **2** (see the Supporting Information). The bands subject to isotopic changes are highly broad,

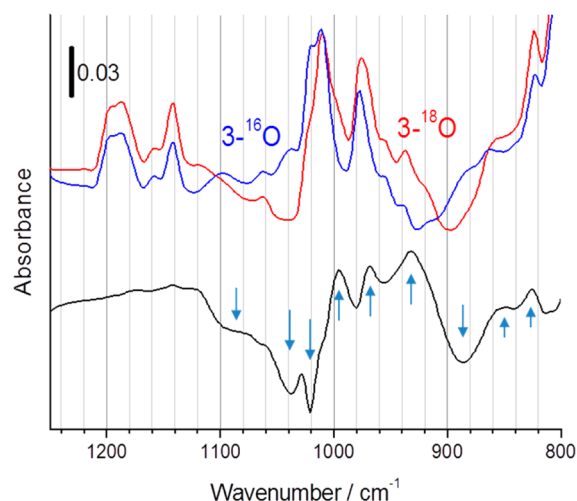


Figure 5. ATR FT-IR spectra of **3** (blue) and **3-¹⁸O** (red) in the region of P–O/P=O stretching vibrations. The bottom spectrum is the difference of the two (**3-¹⁸O** minus **3-¹⁶O**), and the arrows indicate the changes induced by the substitution of ¹⁶O by ¹⁸O.

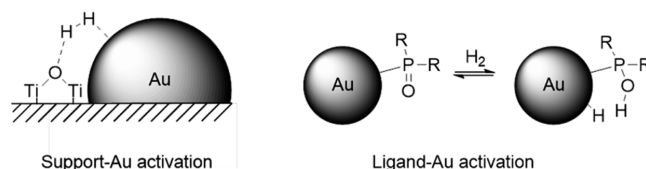
appearing in the whole range of P–O/P=O vibrations, and also multiple, indicating that various configurations and bonding natures of P–O/P=O of **1** exist on the Au nanoparticle and/or the oxygen atom is in contact with other atoms, thereby inducing the shifts in their vibrational frequencies by isotopic substitution. In addition, P=O moieties can coordinate in a μ fashion, connecting two Au atoms.

On the basis of these experiments, we conclude that a Au–P(O)R₂ binding mode is the most likely coordination mode of **1** in **3**. This is somewhat surprising, as in most molecular complexes the preferred bonding mode of SPOs is R₂PO···H···OPR₂, as a monoanionic, H-bonded bidentate diphosphorus ligand. In part this may be for steric reasons; a stable Au₅₀NP needs approximately 30 monoanionic ligands, as in the thiolate clusters, and there is no space for 30 of those bidentate anions.

Catalytic Hydrogenation of Carbonyl Compounds with 3. There are few reports of hydrogenation with Au nanoparticles, and Au is not typically utilized in hydrogenation in nanoparticle, nanocluster, or homogeneous chemistry, in comparison to the typical metals used in hydrogenation chemistry (group 8–10 metals). This is unsurprising, given that Au has been shown to have a very limited capacity to dissociate hydrogen.^{42,43} However, in the cases where activity was observed, Au has shown a surprising preference for the hydrogenation of C=O over C=C bonds and thus merits development.⁴⁴ In light of this, we envisaged Au as an ideal metal to study, as the proposed ligand–metal cooperation does not require a metal-centered redox and has been used extensively in hydrogenation chemistry and elsewhere.⁸ In an initial experiment⁴⁵ we found that exposure of a benzene solution of **3** to an equimolar mixture of H₂ and D₂ (ca. 1 bar) resulted in the formation of HD after standing for ca. 6 h at ambient temperature (Figure S18, Supporting Information), while no scrambling was found to occur in a control experiment containing only **2**. This result clearly demonstrates that hydrogen activation is affected by **3** under very mild conditions. This test has been used in other systems to probe hydrogen dissociation on Au deposited on TiO₂(110), in which the activation is thought to take place at the edges formed between Au and the support.⁴⁶ However, it must be considered that the formation of HD is not necessarily explained by a *heterolytic*

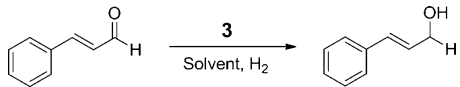
cleavage mechanism involving the ligand and could be envisaged to occur on a plain Au surface. That said, we consider it of particular relevance to draw comparison to the type of mechanism proposed here and those which are proposed to occur at the boundaries between deposited Au nanoparticles and the support (Scheme 2).^{44,47–50}

Scheme 2. Proposed Heterolytic Cleavage of Hydrogen by 3 (Right, This Work) and Comparison with Heterolytic Cleavage of Dihydrogen at the Edges of Au Nanoparticles Supported on Oxide (e.g., TiO₂) Surfaces (Left)



This encouraging demonstration of hydrogen activation motivated us to explore the utility of **3** as a hydrogenation catalyst. Indeed, Jin et al. reported recently that the atomically precise Au₂₅(SR)₁₈ cluster is capable of very selective hydrogenation of α,β -unsaturated aldehydes and ketones under very mild conditions, albeit with a maximum conversion of 54% (TON 16, TOF 5.3 h^{–1}).⁵¹ Inspired by this work, the hydrogenation of a range of α,β -unsaturated aldehydes was examined using catalytic quantities of **3**. Pleasingly, **3** was found to be a highly active and almost exclusively selective catalyst for the hydrogenation of α,β -unsaturated aldehydes. At ambient temperature and 10 bar of H₂ pressure, complete selectivity toward the unsaturated alcohol was observed, albeit with low conversion (Table 1, entry 1, 33%). Increasing the pressure to 40 bar increased the conversion to 54%. Increasing the temperature to 60 °C but with the pressure maintained at 10 bar, gave only a marginal increase in conversion in comparison to ambient temperature (entry 3, 39%). We concluded that the system requires both higher temperatures and H₂ pressures, and quantitative conversion of the substrate to the expected allylic alcohol with 100% selectivity was achieved at 40 bar (entries 3–5).

The solvent was found to be relatively important in that while both THF and hexane consistently gave good results (Table 1, entries 6 and 15–19), other solvents gave lower conversions (entry 7, toluene) or even appeared to poison the catalysis entirely (entry 8, CHCl₃).⁵² Given the anticipated importance of the carbonyl interaction with the catalyst, we were interested in testing the performance of **3** in a carbonyl-containing solvent (entry 9, 2-butanone), anticipating a reduction in efficiency of **3** due to competing coordination of the solvent for the active sites. Surprisingly, in addition to a reduced efficiency we observed a complete loss of selectivity to the α,β -unsaturated alcohol. A significant amount of C=C hydrogenation was observed, and both 3-phenylpropanal (28%) and 3-phenylpropanol (18%) were observed as products in addition to the expected product (cinnamyl alcohol, 8%). This loss of selectivity in carbonyl solvents could provide a clue to the origin of the selectivity in these hydrogenations. Indeed, others have suggested that a C=O→Au interaction is a crucial feature in similar systems.⁵¹ With these optimized reaction parameters, a maximum TON of 1064 (entry 19) and a maximum TOF of 283 h^{–1} (entry 18) were achieved. To the best of our knowledge, this constitutes the best catalytic

Table 1. Optimization Parameters for the Hydrogenation of Cinnamaldehyde Catalyzed by 3^a


entry	[S]/[Au]	solvent	T (°C)	time (h)	P (bar)	conversion (%) ^b
1	50	THF	23	24	10	33
2	50	THF	23	24	40	54
3	50	THF	60	24	10	39
4	50	THF	60	24	20	59
5	50	THF	60	24	30	78
6	50	THF	60	24	40	>95
7	50	toluene	60	24	40	62
8	50	CHCl ₃	60	24	40	0
9	50	2-butanone	60	24	40	54 ^c
10	50	hexane	60	24	40	>95
11	50	THF	60	10	40	>95
12	50	THF	60	5	40	80
13	50	hexane	60	5	40	>95
14	50	hexane	60	1	40	38
15	50	hexane	80	1	40	>95
16	50	hexane	80	0.5	40	>95
17	100	hexane	80	0.5	40	>95
18	213	hexane	80	0.5	40	66.5
19	1064	hexane	60	72	40	>95

^aReagents and conditions: 3 (0.01 mmol Au assuming 46.28% of Au in 3), solvent (5 mL). ^bConversions were determined by ¹H NMR spectroscopy and refer to the selective conversion of cinnamaldehyde (average of two runs). In all cases the only product observable by ¹H NMR spectroscopy was the α,β -unsaturated alcohol. ^cIn this case, the selectivity is drastically altered (vide infra).

performance in terms of rate, catalyst lifetime, and selectivity with unsupported AuNPs to date.⁵³ With optimized reaction conditions in hand, we were keen to demonstrate the substrate scope and functional groups tolerated by 3 (Table 2).⁵⁴ The reaction appears to be very general, and in nearly all cases, very high conversions were observed for a wide range of α,β -unsaturated aldehydes, including some that are of particular interest in the production of perfumes and fragrances.¹⁹ Additionally, essentially perfect chemoselectivity was observed in all cases. Of particular chemical significance is the selective hydrogenation of acrolein to allyl alcohol, which proceeded with perfect selectivity. Although the conversions were consistently lower than those for other substrates, reasonable conversions could be obtained (entry 8, 61%).⁵⁵ In contrast to our system, Jin et al. noted a drop in selectivity when acrolein was used as a substrate (91% at 46% conversion).⁵¹ Notably, no propanal was ever observed by ¹H NMR spectroscopy or GC-MS, which demonstrates that the system is truly selective for C=O over C=C hydrogenation. This result is highly significant, as although Au nanoparticles and supported materials have long since been shown to exhibit an unprecedented selectivity toward hydrogenation of the thermodynamically stronger C=O bond, acrolein represents the most critical demonstration of this selectivity, since both double bonds are essentially isosteric.⁴⁴

In addition to this unprecedented selectivity to C=O over C=C, 3 is also highly tolerant to a wide range of functional groups. For example, although Au is known to hydrogenate nitroaryl compounds,⁵⁶ hydrogenation of *p*-nitrobenzaldehyde

Table 2. Scope of the Reaction^a

Entry	Substrate	Product	Conv. (%) ^b	Selectivity (%)
1	Ph-CHO	Ph-CH ₂ -OH	>95	>99 (A)
2	Ph-CH=CH-CHO	Ph-CH=CH-CH ₂ -OH	>99	>99 (UA) ^f
3	CH ₃ (CH ₂) ₇ -CHO	CH ₃ (CH ₂) ₇ -CH ₂ -OH	94	>99 (A)
4	CH ₃ (CH ₂) ₃ -CH=CH-CHO	CH ₃ (CH ₂) ₃ -CH=CH-CH ₂ -OH	>95 ^d	>99 (UA)
5	CH ₃ -C(CH ₃)=CH-CHO	CH ₃ -C(CH ₃)=CH-CH ₂ -OH	>95 ^d	99:1 (UA:A)
6	CH ₃ -CH=CH-CHO	CH ₃ -CH=CH-CH ₂ -OH	>95 ^d	>99 (UA)
7	CH ₃ -C(CH ₃)=CH-CH ₂ -CHO	CH ₃ -C(CH ₃)=CH-CH ₂ -CH ₂ -OH	>95 ^e	>99 (UA)
8	CH ₂ =CH-CHO	CH ₂ =CH-CH ₂ -OH	61 ^f (22) ^g	>99 (UA) ^f
9	O ₂ N-C ₆ H ₄ -CHO	O ₂ N-C ₆ H ₄ -CH ₂ -OH	>99	>99 (UA)
10	CH ₃ (CH ₂) ₇ -C≡C-CHO	CH ₃ (CH ₂) ₇ -C≡C-CH ₂ -OH	>95	>99 (UA)
11	HC≡C-C ₆ H ₄ -CHO	HC≡C-C ₆ H ₄ -CH ₂ -OH	42	>99 (UA)
12	N≡C-C ₆ H ₄ -CHO	N≡C-C ₆ H ₄ -CH ₂ -OH	90	>99 (UA)
13	Pyridine-2-CHO	Pyridine-2-CH ₂ -OH	86 ^e	>99 (UA)
14	Furan-2-CHO	Furan-2-CH ₂ -OH	94	>99 (UA)
15	Thiophene-2-CHO	Thiophene-2-CH ₂ -OH	>99 ^e	>99 (UA)
16	CH ₃ -C(=O)-C ₆ H ₄ -CHO	CH ₃ -C(=O)-C ₆ H ₄ -CH ₂ -OH	>99	>99 (UA)
17	HOOC-C ₆ H ₄ -CHO	HOOC-C ₆ H ₄ -CH ₂ -OH	>95	>99 (UA)
18	CH ₃ -C(=O)-O-C ₆ H ₄ -CHO	CH ₃ -C(=O)-O-C ₆ H ₄ -CH ₂ -OH	>99	>99 (UA)

^aReagents and conditions: 3 (0.01 mmol Au assuming 46.28% of Au from elemental analysis), substrate (0.5 mmol), THF (5 mL), 18 h, 60 °C, 40 bar of H₂. ^bConversions and product identities were determined by ¹H NMR spectroscopy (average of two runs) and/or GC-MS when appropriate. ^cAfter 4 days of reaction, 2.0% of saturated alcohol was observed. ^dReaction performed at 50 °C. ^eReaction was performed in hexane as solvent. ^fReaction performed at 40 °C. ^gIn neat acrolein. A = alcohol and UA = unsaturated alcohol.

yielded the corresponding nitrobenzyl alcohol with perfect retention of the nitro group (Table 2, entry 9). Similarly, cyano groups (entry 12, 90%) and even reducible sulfur-containing heteroaromatic substituents, esters, and carboxylic acids were also tolerated excellently (entries 15, 17, and 18). Of particular importance is the total inactivity of 3 toward the hydrogenation of ketones, and thus only the aldehyde in 3-acetylbenzaldehyde was hydrogenated with 100% selectivity (entry 16). This is in contrast to other active Au nanoparticles, in which ketones are also hydrogenated.^{13,51} Also noteworthy is the observation that

while internal alkynes were tolerated perfectly (entry 10), we noted a decreased conversion when a terminal alkyne functionality was present (entry 11, 42%). We hypothesized that the terminal alkyne was poisoning the catalyst. In support of this, Tsukuda et al. have described the formation of organogold clusters stabilized by surface Au acetylides obtained by reaction of a terminal alkyne with preformed gold clusters stabilized by PVP,¹⁷ and we hypothesized acetylide for SPO exchange might be the origin of this poisoning. Indeed, we found that hydrogenation of *p*-nitrobenzaldehyde, which usually proceeds quantitatively, in the presence of excess 4-acetylphenylacetylene was completely shut down.

A key attraction to nanoparticle catalysis is the possibility of catalyst recycling. To that end, we carried out a number of experiments using cinnamaldehyde to demonstrate the recyclability of **3**. Ultimately, **3** exhibits a very limited potential for recyclability. Briefly, by removal of the solvent and extraction of both the substrate and products with MeOH followed by subsequent reisololation of the insoluble fraction by centrifugation, **3** could be recovered and used in subsequent reactions. Despite maintenance of perfect chemoselectivity throughout, substantial loss of activity was evident by the third cycle (Figure 6), and we attribute this to both the gradual loss

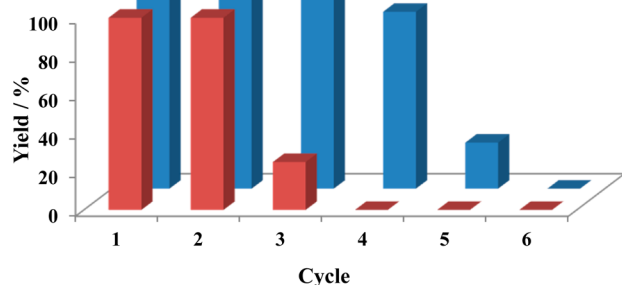


Figure 6. Reuse of **3** in the catalytic hydrogenation of cinnamaldehyde with (red bars) and without (blue bars) separation of catalyst and product. Reagents and conditions: **3** (4 mol %), cinnamaldehyde (0.5 mmol), THF (5 mL), 16 h, 60 °C, 40 bar of H₂.

of **3** upon isolation and/or decomposition due to repeated washing cycles. Greatly improved recyclability was observed when the reaction was performed in batches, simply adding more substrate at the end of the reaction. However, even in this regime a relatively sudden loss of reactivity was observed by the fifth cycle (which corresponds to ca. 5 days at 60 °C). The lack of recyclability of **3** is not surprising, considering **3** is essentially a homogeneous catalyst and isolation involves unavoidable mechanical losses. Although no agglomeration was observed by TEM, we did note a substantial increase in the average size of the particles after one cycle (1.83(0.34) nm, ca. 0.59 nm increase, Figure 7), and this concomitant decrease in surface area is expected to result in a decrease in activity on the basis of available Au. Indeed, Jin et al. noticed a similar unsuitability of Au₂₅(SR)₁₈ to recycling,⁵¹ and we envisage the immobilization of **3** on heterogeneous supports might increase the recyclability. Alternatively, the results could be explained by a stripping of SPO from the surface by aldehydes,⁵⁷ in which case a stronger binding of polydentate SPOs might enhance the catalyst lifetime.

Role of the SPO Ligand in **3.** In order to determine the importance of an SPO ligand in **3** to the observed catalytic activity, we prepared Au nanoparticles via an identical

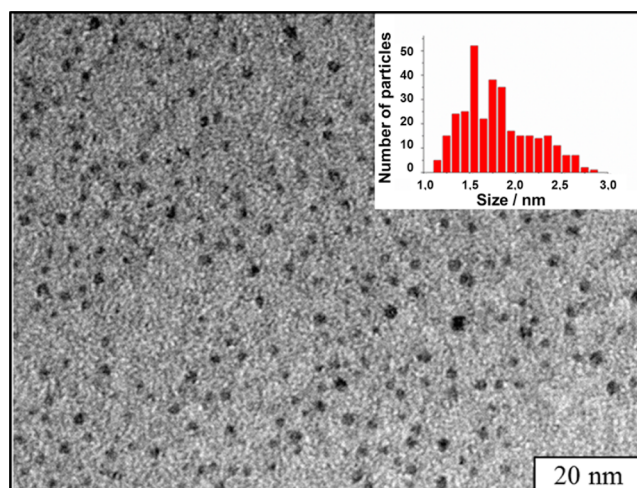
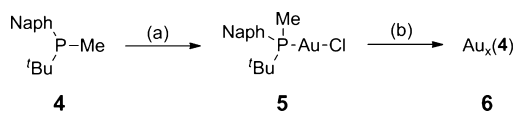


Figure 7. Representative TEM image of **3** after one catalytic run (16 h at 60 °C). The size distribution (inset) was determined from TEM images by counting >300 nontouching particles obtained from images captured from distinct quadrants of the grid.

procedure using the simple tertiary phosphine **4** (Scheme 3). Even though the electron-donor properties of **4** and **1** are not

Scheme 3. Synthesis of Au Nanoparticles (**6**) Stabilized by the Tertiary Phosphine Equivalent **4**^a



^aReagents and conditions: (a) 0.98 equiv of [(tbt)AuCl], DCM, 25 °C, 5 h; (b) 16 equiv of NaBH₄, THF/H₂O (1.4/1), 0–25 °C, 15 h.

directly comparable, **4** serves as a reasonable isosteric equivalent to **1** that is expected to have no capacity for ligand to metal cooperation.⁵⁸ Upon workup (see the Supporting Information) of these particles it was clear that the particles prepared using **4** exhibited very different solubility. That is, although a deeply colored organic fraction was obtained, a large amount of dark purple solid was also isolated from the reaction mixture. Analysis of both the apparently soluble organic phase and precipitate (by dispersion in THF) by TEM revealed that, in both cases, Au nanoparticles of a similar but slightly larger size and greater polydispersity in comparison to **3** (1.46 (0.28) nm) were obtained and it was also apparent that the particles are highly agglomerated in comparison to samples of **3** (Figure 8). In addition to an obvious change in morphology and physical properties, we found that these nanoparticles were completely inactive toward the hydrogenation of cinnamaldehyde (Table 3, entry 4). In a further set of control experiments we found that unstabilized Au metal (entry 1),⁵⁹ the precursor complex **2** (entry 3), and the previously reported Au₁₁ cluster supported by triphenylphosphine⁶⁰ (entry 2) were all totally inactive.

In spite of the fact that there are a few other reports of selective hydrogenation of similar substrates with gold nanoparticles, we conclude that in our system the SPO is critical to the observed reactivity and we speculate that this is related to the aforementioned ligand to metal cooperative effect that can be realized by SPO ligands but not by simple hydrocarbyl phosphines. Generally, the cited mechanism for

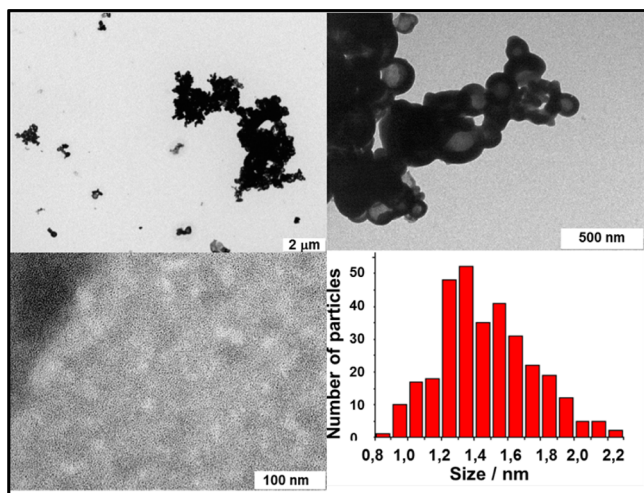


Figure 8. Representative TEM image of AuNPs **6** (from supernatant) and size distribution determined from TEM images.

Table 3. Summary of the Attempted Catalytic Hydrogenation of Cinnamaldehyde using Various Other Sources of Au

entry	catalyst	loading (mol %)	conversion (%) ^b	ref
1	Au	5	0	59
2	Au ₁₁ (PPh ₃) ₇ Cl ₃	2	0	60
3	[^t BuNaphP(OH)AuCl] ₂	2	0	this work
4	Au _x (4) _y	2	0	this work

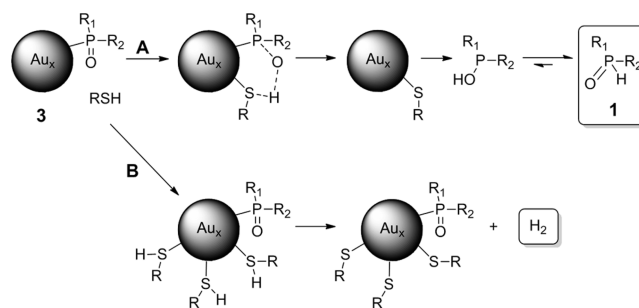
^bReagents and conditions: THF, 25 °C, 5 h, 40 bar of H₂. The reaction mixture was evaluated by removing the volatiles, dissolving the residue in CDCl₃, and analyzing the solution by ¹H NMR spectroscopy.

dihydrogen dissociation by Au involves edges between the metal and oxide support (vide supra); this appears to be the first example where the ligand has been directly implicated in the mechanism of hydrogen activation for homogeneous gold nanoparticles, and it is our view that this widens the scope of hydrogen catalysis using metal–ligand participation substantially.

The implication that **1** is coordinated primarily as an anionic ligand draws parallels between **3** and the closely related thiolate¹⁰ and acetylides¹⁷ clusters. In fact, we envisage that the activation of hydrogen by **3** and thiolate clusters may in fact occur by a related ligand–metal cooperative mechanism (involving protonation of the bound thiolate) rather than purely Au-mediated activation.⁵¹ As a further demonstration of this analogy, we treated a benzene solution of **3** with excess pentanethiol, which resulted in slow (ca. 10 h) exchange of bound **1** to give free **1**, as determined by a loss of the characteristic ¹H NMR resonances attributable to **3** and the appearance of those attributable to **1**⁶¹ along with simultaneous growth of a broad aliphatic signal that we presume to be Au_x(SPent)_y nanoparticles (Scheme 4).

Of particular interest is the observation of dihydrogen by ¹H NMR spectroscopy during this exchange. While we did not attempt to quantify or identify the origin of the dihydrogen,⁶² we hypothesize that **1** is liberated from **3** via protonolysis by pentanethiol (pathway A, Scheme 4) and that the dihydrogen is formed in a reductive type coupling between pentanethiol and

Scheme 4. Possible Mechanisms to Explain the Liberation of **1 Bound at **3** by Pentanethiol and the Appearance of Dihydrogen^a**



^aReagents and conditions: **3** (0.02 mmol), PentSH (0.1 mmol), C₆D₆, 25 °C, ca. 10 h, sealed tube. R₁ = naphthyl, R₂ = *tert*-butyl and R = pentyl.

Au (pathway B, Scheme 4), the mechanism of which is still not fully understood. To the best of our knowledge, although dihydrogen has never been detected in such solution-phase experiments, it is strongly implicated as a byproduct.⁶³

CONCLUSIONS

In summary, we have successfully prepared air-stable AuNPs ligated to strong donor ligands such as secondary phosphine oxides. These types of AuNPs are very active catalysts for the highly chemoselective hydrogenation of substituted aldehydes. High conversions and complete selectivities were obtained with a wide range of α,β -unsaturated aldehydes and very different functional groups (i.e., nitro, cyano, alkynes, heteroaromatic substituents, and other carbonyl groups). This work represents a clear demonstration of the ligand–metal cooperative effect, where the nature of the SPO ligand plays a crucial role and is directly related to the catalytic activity. Furthermore, an extensive characterization of the nanoparticles was performed by several procedures. In particular, we have shown that ATR FT-IR spectroscopy is a powerful tool for the characterization of phosphines directly attached to the AuNP surface, suggesting that the SPO is coordinated as an anionic ligand in the nanoparticles by a Au–P(O)R₂ binding mode. The catalytic properties of AuSPO NPs are not unique for the present ligand **1**, but so far only ligand **1** and particles **3** have been subjected to the detailed study reported here. Studies aimed at exploring the exciting possibility of using P-chiral asymmetric SPOs such as **3** in enantioselective catalysis and obtaining a more complete understanding of the mechanism of this process are currently underway.

ASSOCIATED CONTENT

Supporting Information

Text, figures, tables, and a CIF file giving detailed experimental procedures, analytical and spectral data, and crystallographic data for **2**. This material is available free of charge via the Internet at <http://pubs.acs.org>.

AUTHOR INFORMATION

Corresponding Author

pvanleeuwen@iciq.es

Notes

The authors declare no competing financial interest.

ACKNOWLEDGMENTS

The European Union is acknowledged for an ERC Advanced Grant (NANOSONWINGS 2009-246763). The authors gratefully thank Dr. Jordi Benet-Buchholz for X-ray crystal structure determinations, Dr. Marta Giménez Pedrós, Dr. Yvette Mata Campaña, and Mariona Urtasun Plans for assistance with high-pressure experiments, Maria José Hueso Estornell for GC-MS measurements, and Marta Serrano Torné for technical support. The authors also acknowledge Mercè Moncusí and Dr. Rita Marimon from Universitat Rovira i Virgili for TEM, EDX, and Raman facilities and the Swiss-Norwegian Beamlines at the ESRF for the XRD measurements.

REFERENCES

- (1) Martin, D.; Moraleda, D.; Achard, T.; Giordano, L.; Buono, G. *Chem. Eur. J.* **2011**, *17*, 12729.
- (2) Dubrovina, N. V.; Börner, A. *Angew. Chem., Int. Ed.* **2004**, *43*, 5883.
- (3) It is noted that, in some cases, highly electron withdrawing P substituents shift the equilibrium almost completely in favor of the P(III) species. See ref 4.
- (4) Hoge, B.; Neufeind, S.; Hettel, S.; Wiebe, W.; Thösen, C. J. *Organomet. Chem.* **2005**, *690*, 2382.
- (5) Castro, P. M.; Gulyas, H.; Benet-Buchholz, J.; Bo, C.; Freixa, Z.; van Leeuwen, P. W. N. M. *Catal. Sci. Technol.* **2011**, *1*, 401.
- (6) Jiang, X.-B.; Minnaard, A. J.; Hessen, B.; Feringa, B. L.; Duchateau, A. L. L.; Andrien, J. G. O.; Boogers, J. A. F.; de Vries, J. G. *Org. Lett.* **2003**, *5*, 1503.
- (7) Liniger, M.; Gschwend, B.; Neuburger, M.; Schaffner, S.; Pfaltz, A. *Organometallics* **2010**, *29*, 5953.
- (8) See the following for a variety of examples related to hydrogen activation via ligand–metal cooperation: (a) van Leeuwen, P. W. N. M.; Roobeek, C. F.; Wife, R. L.; Frijns, J. H. G. *J. Chem. Soc., Chem. Commun.* **1986**, 31. (b) Gunanathan, C.; Milstein, D. *Acc. Chem. Res.* **2011**, *44*, 588. (c) Chapman, A. M.; Haddow, M. F.; Wass, D. F. *J. Am. Chem. Soc.* **2011**, *133*, 18463. (d) Askevold, B.; Nieto, J. T.; Tussupbayev, S.; Diefenbach, M.; Herdtweck, E.; Holthausen, M. C.; Schneider, S. *Nat. Chem.* **2011**, *3*, 532. (e) O, W. W. N.; Morris, R. H. *ACS Catal.* **2013**, *3*, 32. (f) Hasanyan, F.; Morris, R. H. *Inorg. Chem.* **2012**, *51*, 10808. (g) Prokopchuk, D. E.; Collado, A.; Lough, A. J.; Morris, R. H. *Dalton Trans.* **2013**, *42*, 10214.
- (9) Rafter, E.; Gutmann, T.; Löw, F.; Buntkowsky, G.; Philippot, K.; Chaudret, B.; van Leeuwen, P. W. N. M. *Catal. Sci. Technol.* **2013**, *3*, 595.
- (10) (a) Brust, M.; Walker, M.; Bethell, D.; Schiffrin, D. J.; Whyman, R. *J. Chem. Soc., Chem. Commun.* **1994**, 7, 801. (b) Woehrlé, G. H.; Warner, M. G.; Hutchison, J. E. *J. Phys. Chem. B* **2002**, *106*, 9979. (c) Woehrlé, G. H.; Hutchison, J. E. *Inorg. Chem.* **2005**, *44*, 6149. (d) Zhu, M.; Lanni, E.; Garg, N.; Bier, M. E.; Jin, R. *J. Am. Chem. Soc.* **2008**, *130*, 1138. (e) Zhu, M.; Aikens, C. M.; Hollander, F. J.; Schatz, G. C.; Jin, R. *J. Am. Chem. Soc.* **2008**, *130*, 5883. (f) Gautier, C.; Bürgi, T. *J. Am. Chem. Soc.* **2008**, *130*, 7077. (g) Lopez-Acevedo, O.; Tsunoyama, H.; Tsukuda, T.; Häkkinen, H.; Aikens, C. M. *J. Am. Chem. Soc.* **2010**, *132*, 8210. (h) Knoppe, S.; Dharmaratne, A. C.; Schreiner, E.; Dass, A.; Bürgi, T. *J. Am. Chem. Soc.* **2010**, *132*, 16783. (i) Pei, Y.; Zeng, X. C. *Nanoscale* **2012**, *4*, 4054. (j) Jung, J.; Kang, S.; Han, Y.-K. *Nanoscale* **2012**, *4*, 4206. (k) Knoppe, S.; Dass, A.; Bürgi, T. *Nanoscale* **2012**, *4*, 4211. (l) Kumar, S.; Jin, R. *Nanoscale* **2012**, *4*, 4222. (m) Negishi, Y.; Kamimura, U.; Ide, M.; Hirayama, M. *Nanoscale* **2012**, *4*, 4263. (n) Yu, Y.; Luo, Z.; Yu, Y.; Lee, J. Y.; Xie, J. *ACS Nano* **2012**, *6*, 7920. (o) Knoppe, S.; Dolamic, I.; Dass, A.; Bürgi, T. *Angew. Chem., Int. Ed.* **2012**, *51*, 7589. (p) Knoppe, S.; Kothalawala, N.; Jupally, V. R.; Dass, A.; Bürgi, T. *Chem. Commun.* **2012**, *48*, 4630. (q) Dolamic, I.; Knoppe, S.; Dass, A.; Bürgi, T. *Nat. Commun.* **2012**, *3*, 798.
- (11) Maity, P.; Xie, S.; Yamauchi, M.; Tsukuda, T. *Nanoscale* **2012**, *4*, 4027.
- (12) Mertens, P. G. N.; Poelman, H.; Ye, X.; Vankelecom, I. F. J.; Jacobs, P. A.; De Vos, D. E. *Catal. Today* **2007**, *122*, 352.
- (13) Mertens, P. G. N.; Vandezande, P.; Ye, X.; Poelman, H.; Vankelecom, I. F. J.; De Vos, D. E. *Appl. Catal., A* **2009**, *355*, 176.
- (14) Vignolle, J.; Tilley, T. D. *Chem. Commun.* **2009**, *46*, 7230.
- (15) (a) Peng, S.; Lee, Y.; Wang, C.; Yin, H.; Dai, S.; Sun, S. *Nano Res.* **2008**, *1*, 229. (b) Ganguly, M.; Pal, A.; Pal, T. *J. Phys. Chem. C* **2012**, *116*, 9265.
- (16) Siddiqui, M. R. H. *J. Chem.* **2013**, *2013*, 4.
- (17) (a) Maity, P.; Tsunoyama, H.; Yamauchi, M.; Xie, S.; Tsukuda, T. *J. Am. Chem. Soc.* **2011**, *133*, 20123. (b) Maity, P.; Wakabayashi, T.; Ichikuni, N.; Tsunoyama, H.; Xie, S.; Yamauchi, M.; Tsukuda, T. *Chem. Commun.* **2012**, *48*, 6085.
- (18) Stefanescu, D.; Glueck, D.; Siegel, R.; Wasylishen, R. *J. Cluster Sci.* **2008**, *19*, 445.
- (19) Herron, N.; Thorn, D. L. *Adv. Mater.* **1998**, *10*, 1173.
- (20) Stefanescu, D. M.; Glueck, D. S.; Siegel, R.; Wasylishen, R. E. *Langmuir* **2004**, *20*, 10379.
- (21) (a) Bartlett, P. A.; Bauer, B.; Singer, S. J. *J. Am. Chem. Soc.* **1978**, *100*, 5085. (b) Schmid, G.; Klein, N.; Korste, L.; Kreibitz, U.; Schönauer, D. *Polyhedron* **1988**, *7*, 605. (c) Weare, W. W.; Reed, S. M.; Warner, M. G.; Hutchison, J. E. *J. Am. Chem. Soc.* **2000**, *122*, 12890. (d) Tamura, M.; Fujihara, H. *J. Am. Chem. Soc.* **2003**, *125*, 15742. (e) Yanagimoto, Y.; Negishi, Y.; Fujihara, H.; Tsukuda, T. *J. Phys. Chem. B* **2006**, *110*, 11611. (f) Bergeron, D. E.; Hudgens, J. W. *J. Phys. Chem. C* **2007**, *111*, 8195. (g) Ha, J.-M.; Solovyov, A.; Katz, A. *Langmuir* **2009**, *25*, 10548. (h) Jewell, A. D.; Sykes, E. C. H.; Kyriakou, G. *ACS Nano* **2012**, *6*, 3545.
- (22) Starkey-Ott, L.; Finke, R. G. *Coord. Chem. Rev.* **2007**, *251*, 1075.
- (23) (a) Sun, K.-Q.; Hong, Y.-C.; Zhang, G.-R.; Xu, B.-Q. *ACS Catal.* **2011**, *1*, 1336. (b) Ren, D.; He, L.; Yu, L.; Ding, R.-S.; Liu, Y.-M.; Cao, Y.; He, H.-Y.; Fan, K.-N. *J. Am. Chem. Soc.* **2012**, *134*, 17592. (c) Zhang, Y.; Cui, X.; Shi, F.; Deng, Y. *Chem. Rev.* **2012**, *112*, 2467. (d) Stratakis, M.; Garcia, H. *Chem. Rev.* **2012**, *112*, 4469. (e) Zhong, R.-Y.; Yan, X.-H.; Gao, Z.-K.; Zhang, R.-J.; Xu, B.-Q. *Catal. Sci. Technol.* **2013**, *3*, 3013.
- (24) Sardar, R.; Shumaker-Parry, J. S. *Chem. Mater.* **2009**, *21*, 1167.
- (25) Hollatz, C.; Schier, A.; Riede, J.; Schmidbaur, H. *J. Chem. Soc., Dalton Trans.* **1999**, *2*, 111.
- (26) Cooling was found to be critical to the formation of small nanoparticles. Reactions conducted at room temperature gave very large, polydisperse samples.
- (27) Moores, A.; Goettmann, F. *New J. Chem.* **2006**, *30*, 1121.
- (28) The complex is at least sparingly soluble in MeOH, since $^{31}\text{P}\{^1\text{H}\}$ and ^1H NMR spectra were acquired in CD_3OD , and thus is effectively removed by repeated washing.
- (29) The elemental ratios were found to be far out from those calculated for both **1** and **2** (taken as reference compounds), and thus we cannot compare the elemental ratios determined for **3** by this method. We attribute this to an abnormally high carbon content (from adventitious carbon of unknown origin). However, the close agreement of both TGA and elemental analysis performed on distinct batches of **3** suggest that these methods provide the correct values. That said, it should be noted that this incorrect calibration has no bearing on the energies of the photoelectron peaks.
- (30) Residue obtained at 1000 °C under a stream of nitrogen. The decomposition of related tertiary phosphine Au nanoparticles has been considered in some detail. See: Schmid, G.; Hess, H. *Z. Anorg. Allg. Chem.* **1995**, *621*, 1147.
- (31) (a) Li, G.; Jin, R. *Acc. Chem. Res.* **2013**, *46*, 1749. (b) Desiredy, A.; Conn, B. E.; Guo, J.; Yoon, B.; Barnett, R. N.; Monahan, B. M.; Kirschbaum, K.; Griffith, W. P.; Whetten, R. L.; Landman, U.; Bigioni, T. P. *Nature* **2013**, *501*, 399.
- (32) In other instances the synthesis of MNPs has been reported to be less reproducible. A detailed comparison of the various elemental ratios of the nanoparticles indicates that the expected elemental ratios for the ligand are not exactly preserved. It is noted that, in many cases, huge and highly variable quantities of solvent are reportedly retained in nanoparticle samples analyzed by elemental analysis. We noted that for

RuNPs prepared from [Ru(COT)(COD)] in THF large increases in the CH content of the isolated nanoparticles were observed. In that case, we demonstrated that this disparity arises from the formation of aliphatic polymeric material by an unknown mechanism involving the decomposition of THF with concomitant generation of water. In the present case, the CH values do not differ substantially and we observe no traces of solvent or polymer formation by HRMAS ¹H NMR or solution-phase NMR. See for example: (a) Axet, M. R.; Castillón, S.; Claver, C.; Philippot, K.; Lecante, P.; Chaudret, B. *Eur. J. Inorg. Chem.* **2008**, 3460. (b) Favier, I.; Massou, S.; Teuma, E.; Philippot, K.; Chaudret, B.; Gomez, M. *Chem. Commun.* **2008**, 3296. (c) Escárcega-Bobadilla, M. V.; Tortosa, C.; Teuma, E.; Pradel, C.; Orejón, A.; Gómez, M.; Masdeu-Bultó, A. M. *Catal. Today* **2009**, 148, 398. (d) González-Gálvez, D.; Nolis, P.; Philippot, K.; Chaudret, B.; van Leeuwen, P. W. N. M. *ACS Catal.* **2012**, 2, 317.

(33) Ramirez, E.; Eradès, L.; Philippot, K.; Lecante, P.; Chaudret, B. *Adv. Funct. Mater.* **2007**, 17, 2219.

(34) Son, S. U.; Jang, Y.; Yoon, K. Y.; Kang, E.; Hyeon, T. *Nano Lett.* **2004**, 4, 1147.

(35) Woehrlé, G. H.; Brown, L. O.; Hutchison, J. E. *J. Am. Chem. Soc.* **2005**, 127, 2172.

(36) Shem, P. M.; Sardar, R.; Shumaker-Parry, J. S. *Langmuir* **2009**, 25, 13279.

(37) Although accurate integration of these broad regions is not possible, as residual solvent signals cannot be avoided, the relative integrals (aromatic:aliphatic) of both the complex (1:1.28) and nanoparticles (1:1.34) are in reasonable agreement.

(38) This can be explained by considering the higher mobility of the protons on the hydrocarbyl substituents. The line shape only marginally improves with MAS, while the rigidly bound P atoms undergo a large narrowing when MAS is applied.

(39) P–OH stretching absorption confirmed by a comparison of the experimental ATR-IR spectrum of **2** and theoretical spectra (Gaussian 09W, B3-LYP, 6-311G(d,p)) of **2** with ¹⁶O and ¹⁸O (see the Supporting Information, Figure S10).

(40) Confirmed by comparison of the isotopic shift between **1** and **1**-²H (see the Supporting Information, Figure S8) by comparison with the calculated spectrum (Gaussian 09W, B3-LYP, 6-311G(d,p)).

(41) Confirmed by comparison of the isotopic shift between **1** and **1**-¹⁸O (see the Supporting Information, Figure S9).

(42) Zanella, R.; Louis, C.; Giorgio, S.; Touroude, R. *J. Catal.* **2004**, 223, 328.

(43) Guzman, J.; Gates, B. C. *Angew. Chem., Int. Ed.* **2003**, 42, 690.

(44) Takei, T.; Akita, T.; Nakamura, I.; Fujitani, T.; Okumura, M.; Okazaki, K.; Huang, J.; Ishida, T.; Haruta, M. In *Advances in Catalysis*; Bruce, C. G., Friederike, C. J., Eds.; Academic Press: New York, 2012; Vol. 55, p 1.

(45) Additionally, we attempted to observe spectroscopic changes in **3** by ¹H and ³¹P{¹H} NMR spectroscopy under 30 bar of H₂ in a high-pressure NMR tube, but no changes were observed.

(46) Fujitani, T.; Nakamura, I.; Akita, T.; Okumura, M.; Haruta, M. *Angew. Chem., Int. Ed.* **2009**, 48, 9515.

(47) Mohr, C.; Hofmeister, H.; Radnik, J.; Claus, P. *J. Am. Chem. Soc.* **2003**, 125, 1905.

(48) Boronat, M.; Illas, F.; Corma, A. *J. Phys. Chem. A* **2009**, 113, 3750.

(49) Bus, E.; Miller, J. T.; van Bokhoven, J. A. *J. Phys. Chem. B* **2005**, 109, 14581.

(50) Noujima, A.; Mitsudome, T.; Mizugaki, T.; Jitsukawa, K.; Kaneda, K. *Angew. Chem., Int. Ed.* **2011**, 50, 2986.

(51) (a) Zhu, Y.; Qian, H.; Drake, B. A.; Jin, R. *Angew. Chem., Int. Ed.* **2010**, 49, 1295. (b) Zhu, Y.; Qian, H.; Zhu, M.; Jin, R. *Adv. Mater.* **2010**, 22, 1915.

(52) This total poisoning by CHCl₃ is likely to be due to deactivation of the catalyst by some unknown reaction with chlorinated solvents. We have noted a similar incompatibility in the Au₁₁ and Au₅₅ phosphine clusters.

(53) For recent reviews, see: (a) Zhang, Y.; Cui, X.; Shi, F.; Deng, Y. *Chem. Rev.* **2012**, 112, 2467. (b) Mikami, Y.; Dhakshinamoorthy, A.;

Alvaro, M.; Garcia, H. *Catal. Sci. Technol.* **2013**, 3, 58. (c) Yuan, Y.; Yao, S.; Wang, M.; Lou, S.; Yan, N. *Curr. Org. Chem.* **2013**, 17, 400.

(54) Although hexane proved to be a more effective solvent during the optimization with cinnamaldehyde, THF was chosen so that all of the substrates examined were totally soluble in the reaction medium.

(55) Due to the volatility of both the reactant and products, an additional control experiment was performed using pure acrolein as solvent (1 mL, 913 equiv). The crude reaction mixture was analyzed directly by ¹H NMR spectroscopy, showing the presence of the corresponding unsaturated alcohol as the sole reaction product (22% conversion, TON = 201) and no trace of 1-propanol.

(56) Grirrane, A.; Corma, A.; García, H. *Science* **2008**, 322, 1661.

(57) Christiansen, A.; Li, C.; Garland, M.; Selent, D.; Ludwig, R.; Franke, R.; Börner, A. *ChemCatChem.* **2010**, 2, 1278 and references cited therein.

(58) We consider that ^tBuNaphP(OMe) may be considered a closer approximation to **1** in terms of electronics; however, such phosphinites are not stable under the (aqueous) reaction conditions and are readily hydrolyzed to the corresponding SPO. For example: Pryjomka, I.; Bartosz-Bechowski, H.; Ciunik, Z.; Trzeciak, A. M.; Ziolkowski, J. *J. Dalton Trans.* **2006**, 1, 213.

(59) Prepared by reduction of [(tth)AuCl] with excess NaBH₄ in ethanol. See the Supporting Information for further details.

(60) Yang, Y.; Chen, S. *Nano Lett.* **2003**, 3, 75.

(61) It should be pointed out that the chemical shifts of **1** in the presence of excess pentanethiol are dramatically altered relative to those of the free ligand. This was confirmed by treating pure **1** with excess pentanethiol in benzene-*d*₆. The spectrum obtained is identical with that obtained in the aforementioned experiment. What is more, removal of the solvent and pentanethiol under vacuum for several hours before redissolution in benzene-*d*₆ gives a spectrum identical with that of pure **1**, proving that no Altherton–Todd type reaction has taken place: Shi, E.; Pei, C. *Synthesis* **2004**, 2995.

(62) Others have tried to interrogate the mechanism of a very closely related exchange reaction between thiols and primary phosphines (anionically bound to gold nanoparticles using deuterium labeling experiments). However, in this case the results were found to be inconclusive due to rapid scrambling reactions between free thiol and free primary phosphines. See ref 18.

(63) See the discussion within articles listed in ref 10.